NANO LETTERS

Subscriber access provided by LAWRENCE BERKELEY NATL LAB

Communication

3-Dimensional Growth of Li2S in Lithium–Sulfur Batteries Promoted by a Redox Mediator

Laura C.H. Gerber, Peter D. Frischmann, Frank Y. Fan, Sean E. Doris, Xiaohui Qu, Angelique Scheuermann, Kristin A. Persson, Yet-Ming Chiang, and Brett A. Helms

Nano Lett., **Just Accepted Manuscript** • DOI: 10.1021/acs.nanolett.5b04189 • Publication Date (Web): 21 Dec 2015

Downloaded from http://pubs.acs.org on December 23, 2015

Just Accepted

"Just Accepted" manuscripts have been peer-reviewed and accepted for publication. They are posted online prior to technical editing, formatting for publication and author proofing. The American Chemical Society provides "Just Accepted" as a free service to the research community to expedite the dissemination of scientific material as soon as possible after acceptance. "Just Accepted" manuscripts appear in full in PDF format accompanied by an HTML abstract. "Just Accepted" manuscripts have been fully peer reviewed, but should not be considered the official version of record. They are accessible to all readers and citable by the Digital Object Identifier (DOI®). "Just Accepted" is an optional service offered to authors. Therefore, the "Just Accepted" Web site may not include all articles that will be published in the journal. After a manuscript is technically edited and formatted, it will be removed from the "Just Accepted" Web site and published as an ASAP article. Note that technical editing may introduce minor changes to the manuscript text and/or graphics which could affect content, and all legal disclaimers and ethical guidelines that apply to the journal pertain. ACS cannot be held responsible for errors or consequences arising from the use of information contained in these "Just Accepted" manuscripts.

ACS Publications

Nano Letters is published by the American Chemical Society. 1155 Sixteenth Street N.W., Washington, DC 20036

Published by American Chemical Society. Copyright © American Chemical Society. However, no copyright claim is made to original U.S. Government works, or works produced by employees of any Commonwealth realm Crown government in the course of their duties.

3-Dimensional Growth of Li_2S in Lithium–Sulfur Batteries Promoted by a Redox Mediator

Laura C. H. Gerber,[†] *Peter D. Frischmann,*[†] *Frank Y. Fan,*[‡] *Sean E. Doris,*[†, ||] *Xiaohui Qu,*[§] *Angelique M. Scheuermann,*[†, ||] *Kristin Persson,*[§, ¶] *Yet-Ming Chiang,*[‡] *Brett A. Helms**[†]

[†] The Molecular Foundry and [§] Computational Research Division, Lawrence Berkeley National Laboratory, One Cyclotron Road, Berkeley, CA 94720, United States

[‡] Department of Materials Science and Engineering, Massachusetts Institute of Technology, Cambridge, MA 02139, United States

[||]Department of Chemistry and [¶]Department of Materials Science and Engineering, University of California, Berkeley, California, 94720, United States

KEYWORDS Lithium-Sulfur Battery, Redox Mediator, Electrodeposition, Polysulfide, morphology, lithium sulfide

ABSTRACT During the discharge of a lithium-sulfur (Li–S) battery, an electronically insulating 2D layer of Li_2S is electrodeposited onto the current collector. Once the current collector is enveloped, the overpotential of the cell increases and its discharge is arrested, often before reaching the full capacity of the active material. Guided by a new computational platform

known as the Electrolyte Genome, we advance and apply benzo[*ghi*]peryleneimide (BPI) as a redox mediator for the reduction of dissolved polysulfides to Li_2S. With BPI present, we show that it is now possible to electrodeposit Li_2S as porous, 3D deposits onto carbon current collectors during cell discharge. As a result, sulfur utilization improved 220% due to a 6-fold increase in Li_2S formation. To understand the growth mechanism, electrodeposition of Li_2S was carried out under both galvanostatic and potentiostatic conditions. The observed kinetics under potentiostatic conditions were modeled using modified Avrami phase transformation kinetics, which showed that BPI slows the impingement of insulating Li_2S islands on carbon. Conceptually, the pairing of conductive carbons with BPI can be viewed as a vascular approach to the design of current collectors for energy storage devices: here, conductive carbon "arteries" dominate long-range electron transport, while BPI "capillaries" mediate short-range transport and electron transfer between the storage materials and the carbon electrode.

Promising next-generation battery chemistries, including lithium-sulfur (Li–S)[1–4] and lithium-air ($Li–O_2$),[5–8] rely on dissolution-precipitation as a mechanism to release and store charge in the cathode. In both cases, the discharge products are electronically insulating[9–13] (absent defects in the deposits[14–16]). The insulating nature of these deposits can contribute to poor rate capability, low active-material utilization, and high polarization, which reduce overall energy efficiency.[17–19] Charge-transport and charge-transfer bottlenecks in these electrochemical cells are eased through the use of electronically-conductive, high surface-area electrodes;[20–29] many electrode architectures have been reported yielding high-performance $Li–O_2$ cells,[30–33] composite sulfur cathodes[34–37] and flowable sulfur catholytes for redox flow batteries[38–40].

Despite these advances, challenges remain in controlling the electrodeposition of the electronically-insulating solid phase (i.e., Li_2S for Li–S cells, and Li_2O_2 for Li–O_2 cells) to maintain an accessible electrode surface, which is critical to cell performance.

Here we show that Li_2S electrodeposition on carbon current collectors can be redirected away from thin 2D layers, and instead toward micron-sized, porous 3D deposits when benzo[*ghi*]peryleneimide (BPI) is present as a redox mediator (Figure 1). Key to the design of the redox mediator is that the reduction potential of BPI is slightly less than the plateau voltage where the reduction of $Li_2S_4 \rightarrow Li_2S$ occurs. When BPI is reduced at the electrode surface and given time to diffuse away, it can reduce dissolved polysulfides to Li_2S remotely. With BPI present in the electrolyte, a 6-fold increase in Li_2S formation capacity was observed, leading to an impressive 220% increase in overall sulfur utilization. *Ex situ* analysis of Li_2S electrodeposition at different stages of discharge showed divergent trajectories for Li_2S nucleation and growth in the absence *vs.* presence of BPI. Kinetic studies linked the increased sulfur utilization to BPI's ability to slow the impinging growth of Li_2S on the carbon electrode. By pairing conductive carbons with organic redox mediators, we gain access to hierarchical electrodes reminiscent of biological vasculature,[41–45] where conductive carbon "arteries" facilitate long-range electron transport while BPI "capillaries" mediate short-range transport and electron transfer between the storage materials and the current collector.

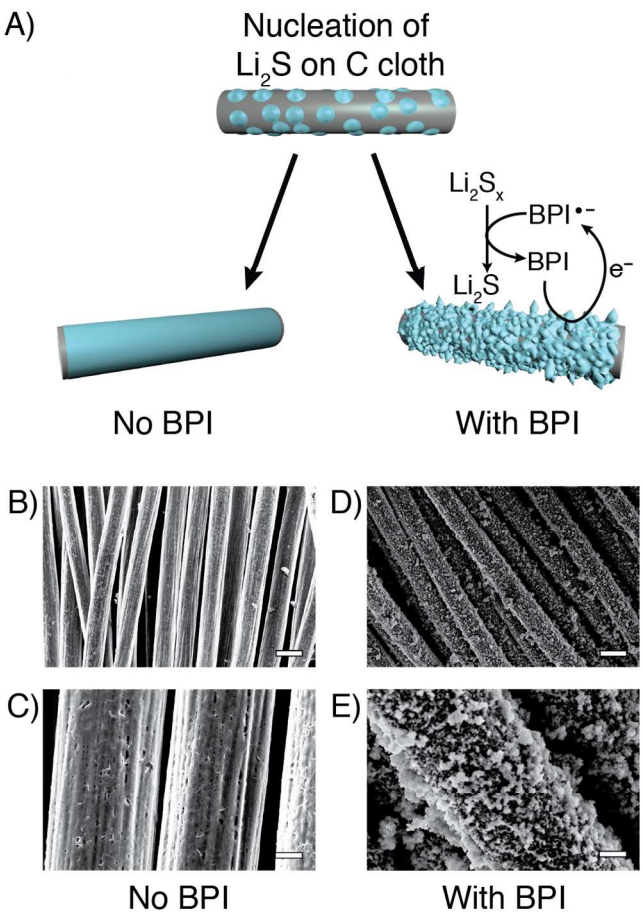

Figure 1. A) Schematic representation of the electrodeposition of Li_2S onto C cloth in the absence (left) and presence (right) of the redox mediator, BPI. B) and C) Scanning electron micrographs of Li_2S deposited on C cloth after battery discharge without BPI. D) and E) SEM micrographs of Li_2S deposited on C cloth after battery discharge with BPI redox mediator The scale bars are in 10 μm B) and D) and 2 μm and C) and E).

While soluble redox mediators have been explored widely for metal-air batteries,[46–52] their application in Li–S batteries is still nascent. The redox chemistry of sulfur in Li–S cells is observed as two electrochemically distinct steps, a low-potential event ~2.1 V *vs.* Li/Li^+

attributed to the interconversion of Li_2S_4 and Li_2S and a high-potential event ~2.5 V *vs.* Li/Li^+ attributed to the interconversion of S_8 and Li_2S_4.[53–57] Paramount to the design of any redox mediator for Li–S cells is the careful matching of the mediator's electrochemical potential to either of these interconversion events. With respect to the former, Aurbach *et al.* have shown that redox mediators can lower the overpotential required for the initial activation of solid-state Li_2S cathodes.[58] With respect to the latter, we have recently reported that perylene bisimides (PBI) serve as redox mediators for the high-voltage plateau. While sulfur utilization was enhanced by 31%,[45] this voltage window represents only 25% of the total theoretical capacity of sulfur. Therefore in this work, our focus turned to identifying a redox mediator for the 2.1 V (*vs.* Li/Li^+) reduction event, where Li_2S_4 reduction results in Li_2S precipitation onto the current collector. Although three-quarters of the theoretical capacity of sulfur is gained in this region, there are no reported redox mediators to facilitate Li_2S electrodeposition.

Our discovery of BPI as a redox mediator for Li_2S electrodeposition was informed by a robust computational platform known as the Electrolyte Genome that allowed us to screen the redox chemistry of polycyclic aromatic hydrocarbons (PAHs). PAHs are ideal redox mediators, owing to an exceptionally low reorganization energy required for their reduction and oxidation.[59–61] In our previous work, we screened the electron affinities (E_{ea}) and ionization potentials (E_i) of over 80 PAHs—including acenes, phenylenes, rylenes, coronenes, and benzoperylenes.[45] This library helped us identify PAHs with imide substituents that could be further elaborated upon to tune the E_{ea} so these molecules can serve as redox mediators for Li_2S electrodeposition. To refine the library and understand how the number and placement of imide functional groups would impact E_{ea}, a focused library of 20 additional PAH molecules was screened to hone in on a structure with a reduction potential (E_{ea}) of ~1.8–2.0 V *vs.* Li/Li^+. This

reduction potential was targeted because it would provide sufficient driving force for Li_2S formation without sacrificing cell power.

Electron affinities were obtained from the calculated energy difference between the neutral and the anion state of the molecule. All calculations were performed at the M11/6-31+G*/PBE-D3/6-31+G* level,[62,63] which has previously been shown to yield reliable relative trends for redox potentials across thousands of molecules (for more details, see SI).[64,65] Trends from the computational results show that increasing the size of the aromatic core from perylene to benzoperylene to coronene lowers the reduction potential from 1.07 to 0.78 to 0.50 V *vs.* Li/Li^+. On the other hand, increasing the number of electron-withdrawing groups raises the reduction potential; the addition of one imide substituent raises the reduction potential >0.9 V, and additional imide substituents beyond that increase E_{ea} by an additional 0.5 V at most. In general, the placement of the electron-withdrawing imide substituents around the PAH core results in only small differences in E_{ea}. By balancing the effects of the size of aromatic core and number of electron-withdrawing groups, several candidates were found with calculated E_{ea} values between 1.8 and 2.0 V *vs.* Li/Li^+ (Figure S1). Due to its synthetic accessibility, the BPI structure was chosen for further study (Figure 2A).

Guided by these predictions from the Electrolyte Genome, we designed and synthesized gram-scale quantities of a new *N*-aryl-substituted benzo[*ghi*]peryleneimide (BPI, Scheme S1) bearing two tri(ethylene oxide) substituents. These substituents provided for BPI solubility in ether-based electrolytes commonly used in Li–S cells. Owing to the single imide substituent, BPI undergoes a single electron reduction in the operating window of the Li–S battery (1.8–2.8 V *vs.* Li/Li^+), leading to an open-shell radical anion ($BPI^{\bullet-}$). Using cyclic voltammetry in diglyme-based electrolyte, we determined the reduction potential ($E_{1/2}$) of BPI to be 1.980 V *vs.* Li/Li^+

(Figure 2B, orange trace), which agreed well with the calculated value of 1.99 V *vs.* Li/Li^+ when a Li^+ counter-ion was included in the calculation (Figure S1). Thus, BPI provides ~100 mV driving force for the reduction of sulfur species. This small overpotential ensures that BPI should be able to reduce all sulfur species to Li_2S, but is not expected to significantly lower the operating voltage of the Li–S cell.

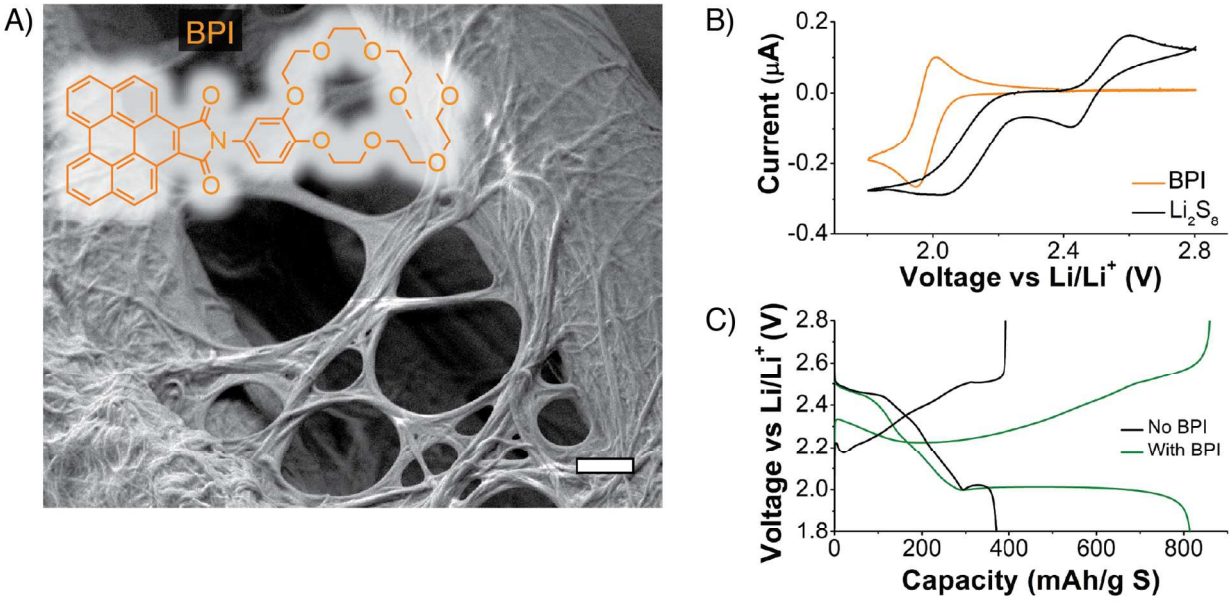

Figure 2. A) Chemical structure of the redox mediator BPI (*inset*) and SEM micrograph of BPI dropcast onto C cloth and dried under vacuum. Scale bar = 2 μm. B) Cyclic voltammograms of BPI (*orange trace*, 2.5 mM BPI) and Li_2S_8 (*black trace*, 12 mM sulfur) at 1 mV s^{-1}. The electrolyte is 0.50 M LiTFSI and 0.15 M $LiNO_3$ in diglyme, with a glassy C working electrode and lithium reference and counter electrodes. C) Second cycle discharge and charge profiles of

Li–S cells at a C/8 rate in the absence (*black trace*) or presence (*green trace*) of BPI redox mediator.

BPI can be introduced to Li-S cells by dissolution in the electrolyte or by dropcasting onto C cloths (3% *w/w* BPI with respect to the sulfur catholyte), with similar results. Our implementation of C cloth electrodes, which feature 8 micron-thick carbon fibers, were chosen because they allow for careful visualization of Li_2S electrodeposition throughout the battery's operation. A hierarchical morphology of the BPI-C cloth hybrid in the dry state was apparent in the scanning electron micrograph (Figure 2A) where BPI assemblies, microns in length and formed through π-stacking of the aromatics, both covered and traversed the larger-diameter carbon fibers. Once polysulfide-containing electrolyte is added, these nanowire assemblies are expected to dissolve and circulate into the electrolyte volume, with the persistence length of the assemblies considerably shortened.[66,67]

To ascertain whether BPI has an affect on Li_2S electrodeposition, galvanostatic cycling was carried out on Li–S cells (Swagelok type) prepared with dissolved polysulfide cathodes alongside C cloth electrodes either with or without BPI. In the absence of BPI, the first complete discharge capacity was 316 ± 18 mAh g^{-1} S (N = 16). On the other hand, with BPI present (3% *w/w* with respect to catholyte), the capacity increased to 691 ± 18 mAh g^{-1} S (N =16). This corresponds to an impressive 2.2-fold increase in discharge capacity (Figure 2C). Notably, this increase in capacity was due to a greatly extended 2.0 V-plateau, indicative of increased Li_2S formation as would be predicted for BPI were it serving as a redox mediator. No difference in cell performance was observed when BPI was introduced to the system by dissolution in the

electrolyte as opposed to dropcasting on C cloth. Cells with dissolved BPI show a discharge capacity of 696 ± 41 mAh g^{-1} S (N = 7), indicating that BPI on the C surface is not simply serving as a nucleation point for Li_2S. Further experiments were conducted with the BPI dropcast onto C cloth for ease of cell assembly.

To quantify the respective gains in capacity between the high- and low-voltage regimes, we divided the discharge curve between the soluble regime ($S_8 + 4\ Li^+ + 4\ e^- \rightarrow 2\ Li_2S_4$) and the Li_2S precipitation plateau ($Li_2S_4 + 6\ Li^+ + 6\ e^- \rightarrow 4\ Li_2S$) at the position of the dip in the discharge curves at ~2.0 V in Figure 2C, which is attributed to the overpotential required for nucleation of Li_2S.[68] The average capacities for the soluble regime are essentially identical (within error): 242 ± 18 mAh g^{-1} S without BPI and 250 ± 18 mAh g^{-1} S with BPI. However, the average capacity for Li_2S electrodeposition was 446 ± 12 mAh g^{-1} S with BPI present, whereas it was only 74 ± 2 mAh g^{-1} S for cells lacking BPI. Thus, the presence of BPI redox mediator resulted in a 6-fold increase in Li_2S electrodeposition. Additional control experiments confirmed that both redox mediator and C cloth are essential for the observed enhancement in sulfur utilization (Figure S4). Battery rate tolerance (Figure S5) and cycling data (Figures S6 and S7) are shown in the Supporting Information.

In order to better understand nucleation and growth of Li_2S on C cloth with BPI present, we carried out *ex situ* analysis of Li–S cells at different states-of-charge (SOC). At specified points along the discharge and recharge (Figure 3A), we disassembled the cells, retrieved the C cloth from those cells, washed away the electrolyte containing salts, polysulfides and BPI, and then imaged the Li_2S discharge products using scanning electron microscopy (SEM); we also collected energy-dispersive x-ray (EDX) spectra of those samples to verify the chemical identity of the discharge products. Upon nucleation (Figure 3A, Point 1), small islands of Li_2S were

distributed over the C microfibers both when BPI was present (Figure 3F) and absent (Figure 3B) from the cell. The presence of a soluble redox mediator is not expected to change Li_2S nucleation, and does not appear to do so here. With BPI present, a globular Li_2S morphology started to form (Figure 3G) mid-way though the 2.0 V plateau (Point 2), yet the underlying C cloth remained visible. On the other hand, without BPI present, islands of Li_2S began to impinge (Figure 3C), leaving little of the C surface available for further redox chemistry with dissolved polysulfides. By the end of discharge (Point 3), the carbon cloth from the cells with BPI showed even larger, porous Li_2S deposits, up to 3.8 μm, growing outward until the underlying carbon cloth current collector was no longer visible (Figure 3H). EDX spectra were consistent with the assignment as Li_2S or insoluble polysulfide species (Table S1). These porous 3D growths of Li_2S at the end of the discharge were substantively different from the thin, conformal coatings observed when BPI was absent (Figure 3C)—such conformal coatings are consistent with previous studies.[68] A similar change in morphology of Li_2O_2 has been observed when a soluble redox mediator is used in Li-air cells.[51] Upon charging to 100% SOC (Point 4), scant Li_2S remains on either carbon surface, without or with BPI added, as expected after complete oxidation of Li_2S (Figure 3E and 3I, respectively).

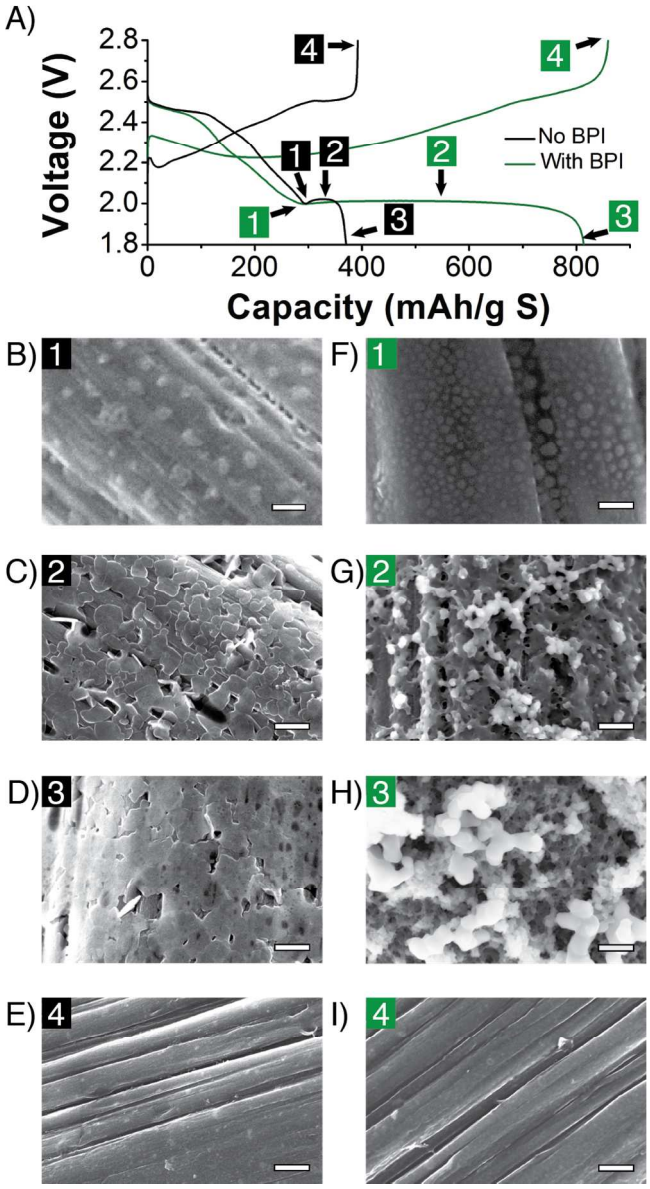

Figure 3. Progressive electrodeposition of Li_2S on C cloth, imaged at different states-of-charge in Li–S cells with BPI absent (left) and BPI present (right) A) The first discharge/charge cycle at C/8 rate. States-of-charge are indicated as Points 1–4 where separate cells were stopped to image the Li_2S deposits on the C cloth. SEM images of Li_2S electrodeposition on C cloth from a cell without BPI are shown: B) at nucleation (Point 1); C) during the Li_2S voltage plateau (Point 2); D) at the end of discharge (Point 3); and E) after recharge (Point 4). SEM images of Li_2S

electrodeposition on C cloth from a cell with BPI: F) at nucleation (Point 1); G) during the Li_2S voltage plateau (Point 2); H) at the end of discharge (Point 3); and I) after recharge (Point 4). Scale bars = 500 nm.

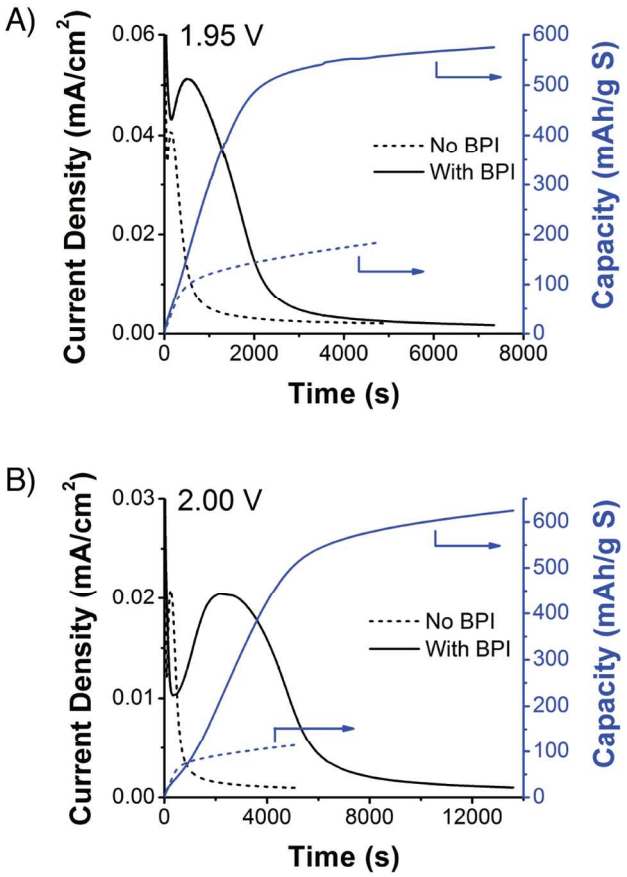

Figure 4. Current transients during the potentiostatic deposition of Li_2S on C cloth. Cells were first discharged to 2.09 V, and the time plot starts upon lowering the voltage to 1.95 V (A) or 2.00 V (B). Solid lines indicate cells containing BPI and dashed lines indicate cells without BPI. Current densities are shown in black and capacities are shown in blue.

The growth trajectory of these 3D deposits involves reduction of BPI at the C cloth surface, followed by diffusion and circulation of $BPI^{\bullet-}$ into the catholyte solution where it reduces polysulfides to Li_2S which can deposit onto either Li_2S or C surfaces resulting in the observed 3D morphologies. This process is competitive with the direct reduction of polysulfides at the electrode surface, which instead coats the C surface in thin conformal layers. To understand the relative rates of these competitive processes, we further studied these Li–S cells under potentiostatic discharge. To do so, the cells were initially discharged potentiostatically to 2.09 V to reduce all S_8 and higher order polysulfides to Li_2S_4 (nominally), in order to study only the electrodeposition of Li_2S. The current was then monitored over time upon lowering the potential to either 2.00 or 1.95 V to provide a driving force for Li_2S nucleation and growth (Figure 4). In both cases, the current trended towards 0 whether or not BPI was present, which indicated that sulfur utilization is ultimately limited by impingement of insulating Li_2S blocking the carbon surface. If Li_2S were to continue to be reduced after the electronically conductive C cloth surface were covered, a horizontal asymptote would instead be expected at a current density > 0 mA cm^{-2}. At 1.95 V, the current density peaks at a higher value and at a later time when BPI is included, leading to a 3.1-fold increase in capacity due to Li_2S deposition (Figure 4A). At 2.00 V, while the cell with BPI does not obtain a higher current density than without BPI, this current density is maintained for much longer when BPI is present, leading to a 5.5-fold increase in capacity due to Li_2S deposition (Figure 4B).

The potentiostatic electrodeposition of Li_2S was fit by a current density (J) *vs.* time (t) relation of the form:

$$\frac{J}{J_m} = \left(\frac{t}{t_m} + c\right) exp\left[-\frac{1}{2}\left(\frac{t^2}{t_m^2} - 1\right)\right] \quad (1)$$

where J_m and t_m are the maximum current density and the time at which the maximum current density occurs, respectively.[69,70] Equation 1 is a modified form of the Avrami equation that models instantaneous nucleation of Li_2S and growth of islands to impingement. The exponential term represents the probability that a given area of the electrode remains uncovered by Li_2S and is therefore available for reaction. The term c accounts for additional current due to the redox mediator; when no redox mediator is present $c = 0$, but this term is required when BPI is present ($c = 1.24$ at 1.95 V and $c = 0.14$ at 2.00 V). This model fits the data both with and without redox mediator, indicating that in both cases the current is proportional to the remaining free surface of carbon. This implies that both with and without redox mediator, impingement of insulating Li_2S deposits covering the carbon surface ended discharge prior to reaching the theoretical limit; however, the addition of BPI redox mediator dramatically enhanced sulfur utilization prior to impingement.

The width of the peak fit by equation 1 can be used to determine the rate constant of lateral growth of Li_2S, k (where lateral growth is the disappearance of C surface available for reaction).

$$t_m = (2\pi N_0 k^2)^{-1/2} \quad (2)$$

where N_0 is the areal density of nuclei. The term N_0k^2 can be compared as an effective rate constant for coverage of the C cloth surface by Li_2S. Without redox mediator, $N_0k^2 = 4.21 \times 10^{-6}$ s^{-2} and 2.52×10^{-6} s^{-2}, at 1.95 and 2.00 V, respectively, and with redox mediator, $N_0k^2 = 1.51 \times 10^{-7}$ s^{-2} and 2.35×10^{-8} s^{-2}, at 1.95 and 2.00 V, respectively. Addition of BPI results in a 28-fold reduction in the coverage rate at 1.95 V and a 107-fold reduction at 2.00 V. In both cases, having the soluble redox mediator slows the coverage of C cloth surface by allowing deposition of Li_2S

onto previously formed Li_2S and not just at the carbon surface. The coverage of the C surface is likely slowed by (1) direct competition between BPI and polysulfides for reduction at the carbon surface, and (2) $BPI^{\bullet-}$ intercepting incoming soluble polysulfides and reducing them to Li_2S away from the C cloth surface, effectively lowering the local concentration of polysulfide at the carbon surface.

In conclusion, with a redox mediator that is tuned to the potential of Li_2S electrodeposition, we are able to mitigate the limitations imposed by the surface area required for nucleation and growth of Li_2S by providing a new mechanism for Li_2S deposition. Both the potentiostatic and galvanostatic discharge experiments confirm that the addition of 3% (*w/w*) BPI redox mediator increases the amount of Li_2S produced 6-fold. By adding an equivalent mass of C cloth, only an additional 24 mAh/g S could be added to the capacity, based on the additional surface area available for 2D deposition of Li_2S. Without BPI, polysulfides are reduced at the C cloth surface to form an insulating, conformal coating of Li_2S, but with redox mediator, BPI reduces polysulfides to Li_2S away from the surface, allowing deposition of Li_2S not only on the C cloth surface, but on previously deposited Li_2S. This forms porous, 3-dimensional structures of Li_2S and delays coverage of the electroactive C cloth with an insulating Li_2S layer that ends discharge. This implies that for a given amount of Li_2S formed during cycling, less conductive carbon additive should be required, allowing for a greater percentage of the battery to be dedicated to active material. With an understanding of the mechanism by which BPI redox mediator extends sulfur utilization, rapid development of Li–S cells with an increased energy density is underway though the integration of BPI with high surface area current collectors at high sulfur loadings.

Supporting Information. Synthesis, characterization, and experimental details. This material is available free of charge via the Internet at http://pubs.acs.org

Corresponding Author

*BAHelms@lbl.gov

Author Contributions

The manuscript was written through contributions of all authors. All authors have given approval to the final version of the manuscript.

Notes

The authors declare no competing financial interest.

ACKNOWLEDGMENT

This work was supported by the Joint Center for Energy Storage Research, an Energy Innovation Hub funded by the U.S. Department of Energy, Office of Science, Office of Basic Energy Sciences. Portions of the work—including BPI synthesis, characterization, and experimental validation as a redox mediator in Li–S cells—were carried out as a user project at the Molecular Foundry, which is supported by the Office of Science, Office of Basic Energy Sciences, of the U.S. Department of Energy under contract no. DE-AC02-05CH11231. This research used resources of the National Energy Research Scientific Computing Center, a DOE Office of Science User Facility supported by the Office of Science of the U.S. Department of Energy under Contract No. DE-AC02-05CH11231. S.E.D. was supported by the Department of Defense through the National Defense Science & Engineering Graduate Fellowship Program.

REFERENCES

(1) Dunn, B.; Kamath, H.; Tarascon, J.-M. *Science* **2011**, *334*, 928–935.

(2) Yin, Y.-X.; Xin, S.; Guo, Y.-G.; Wan, L.-J. *Angew. Chem. Int. Ed.* **2013**, *52*, 13186–13200.

(3) Manthiram, A.; Fu, Y.; Chung, S.-H.; Zu, C.; Su, Y.-S. *Chem. Rev.* **2014**, *114*, 11751–11787.

(4) Evers, S.; Nazar, L. F. *Acc. Chem. Res.* **2013**, *46*, 1135–1143.

(5) Black, R.; Adams, B.; Nazar, L. F. *Adv. Energy Mater.* **2012**, *2*, 801–815.

(6) Girishkumar, G.; McCloskey, B.; Luntz, A. C.; Swanson, S.; Wilcke, W. *J. Phys. Chem. Lett.* **2010**, *1*, 2193–2203.

(7) Christensen, J.; Albertus, P.; Sanchez-Carrera, R. S.; Lohmann, T.; Kozinsky, B.; Liedtke, R.; Ahmed, J.; Kojic, A. *J. Electrochem. Soc.* **2012**, *159*, R1–R30.

(8) Gallagher, K. G.; Goebel, S.; Greszler, T.; Mathias, M.; Oelerich, W.; Eroglu, D.; Srinivasan, V. *Energy Environ. Sci.* **2014**, *7*, 1555–1563.

(9) Radin, M. D.; Siegel, D. J. *Energy Environ. Sci.* **2013**, *6*, 2370–2379.

(10) Viswanathan, V.; Thygesen, K. S.; Hummelshøj, J. S.; Nørskov, J. K.; Girishkumar, G.; McCloskey, B. D.; Luntz, A. C. *J. Chem. Phys.* **2011**, *135*, 214704–214710.

(11) Albertus, P.; Girishkumar, G.; McCloskey, B.; Sánchez-Carrera, R. S.; Kozinsky, B.; Christensen, J.; Luntz, A. C. *J. Electrochem. Soc.* **2011**, *158*, A343–A351.

(12) Rauh, R. D.; Abraham, K. M.; Pearson, G. F.; Surprenant, J. K.; Brummer, S. B. *J. Electrochem. Soc.* **1979**, *126*, 523–527.

(13) Yang, Y.; Zheng, G.; Misra, S.; Nelson, J.; Toney, M. F.; Cui, Y. *J. Am. Chem. Soc.* **2012**, *134*, 15387–15394.

(14) Lu, Y.-C.; Gallant, B. M.; Kwabi, D. G.; Harding, J. R.; Mitchell, R. R.; Whittingham, M. S.; Shao-Horn, Y. *Energy Environ. Sci.* **2013**, *6*, 750–768.

(15) Hummelshøj, J. S.; Blomqvist, J.; Datta, S.; Vegge, T.; Rossmeisl, J.; Thygesen, K. S.; Luntz, A. C.; Jacobsen, K. W.; Nørskov, J. K. *J. Chem. Phys.* **2010**, *132*, 071101–071104.

(16) Radin, M. D.; Monroe, C. W.; Siegel, D. J. *Chem. Mater.* **2015**, *27*, 839–847.

(17) Cheon, S.-E.; Ko, K.-S.; Cho, J.-H.; Kim, S.-W.; Chin, E.-Y.; Kim, H.-T. *J. Electrochem. Soc.* **2003**, *150*, A796–A799.

(18) Barchasz, C.; Leprêtre, J.-C.; Alloin, F.; Patoux, S. *J. Power Sources* **2012**, *199*, 322–330.

(19) Read, J. *J. Electrochem. Soc.* **2002**, *149*, A1190–A1195.

(20) Zhang, K.; Hu, Z.; Chen, J. *J. Energy Chem.* **2013**, *22*, 214–225.

(21) Tao, X.; Wang, J.; Ying, Z.; Cai, Q.; Zheng, G.; Gan, Y.; Huang, H.; Xia, Y.; Liang, C.; Zhang, W.; Cui, Y. *Nano Lett.* **2014**, *14*, 5288–5294.

(22) Pang, Q.; Kundu, D.; Cuisinier, M.; Nazar, L. F. *Nat. Commun.* **2014**, *5*, 4759.

(23) Liang, X.; Garsuch, A.; Nazar, L. F. *Angew. Chemie Int. Ed.* **2015**, *54*, 3907–3911.

(24) Wang, J.; Yang, J.; Wan, C.; Du, K.; Xie, J.; Xu, N. *Adv. Funct. Mater.* **2003**, *13*, 487–492.

(25) Chen, H.; Zou, Q.; Liang, Z.; Liu, H.; Li, Q.; Lu, Y.-C. *Nat. Commun.* **2015**, *6*, 5877.

(26) Yang, X.-H.; He, P.; Xia, Y.-Y. *Electrochem. commun.* **2009**, *11*, 1127–1130.

(27) Kuboki, T.; Okuyama, T.; Ohsaki, T.; Takami, N. *J. Power Sources* **2005**, *146*, 766–769.

(28) Tran, C.; Yang, X.-Q.; Qu, D. *J. Power Sources* **2010**, *195*, 2057–2063.

(29) Xiao, J.; Wang, D.; Xu, W.; Wang, D.; Williford, R. E.; Liu, J.; Zhang, J.-G. *J. Electrochem. Soc.* **2010**, *157*, A487–A492.

(30) Abraham, K. M.; Jiang, Z. *J. Electrochem. Soc.* **1996**, *143*, 1–5.

(31) Mitchell, R. R.; Gallant, B. M.; Thompson, C. V.; Shao-Horn, Y. *Energy Environ. Sci.* **2011**, *4*, 2952–2958.

(32) Xiao, J.; Mei, D.; Li, X.; Xu, W.; Wang, D.; Graff, G. L.; Bennett, W. D.; Nie, Z.; Saraf, L. V; Aksay, I. A.; Liu, J.; Zhang, J.-G. *Nano Lett.* **2011**, *11*, 5071–5078.

(33) Wang, Y.; Zhou, H. *J. Power Sources* **2010**, *195*, 358–361.

(34) Wang, J. L.; Yang, J.; Xie, J. Y.; Xu, N. X.; Li, Y. *Electrochem. Commun.* **2002**, *4*, 499–502.

(35) Ji, X.; Lee, K. T.; Nazar, L. F. *Nat. Mater.* **2009**, *8*, 500–506.

(36) Manthiram, A.; Fu, Y.; Su, Y. *Acc. Chem. Res.* **2013**, *46*, 1125–1134.

(37) Yang, Y.; Zheng, G.; Cui, Y. *Chem. Soc. Rev.* **2013**, *42*, 3018–3032.

(38) Fan, F. Y.; Woodford, W. H.; Li, Z.; Baram, N.; Smith, K. C.; Helal, A.; McKinley, G. H.; Carter, W. C.; Chiang, Y. M. *Nano Lett.* **2014**, *14*, 2210–2218.

(39) Chen, H.; Zou, Q.; Liang, Z.; Liu, H.; Li, Q.; Lu, Y.-C. *Nat. Commun.* **2015**, *6*, 5877.

(40) Yang, Y.; Zheng, G.; Cui, Y. *Energy Environ. Sci.* **2013**, *6*, 1552–1558.

(41) Toohey, K. S.; Sottos, N. R.; Lewis, J. A.; Moore, J. S.; White, S. R. *Nat. Mater.* **2007**, *6*, 581–585.

(42) Nguyen, D. T.; Leho, Y. T.; Esser-Kahn, A. P. *Lab Chip* **2012**, *12*, 1246.

(43) Esser-Kahn, A. P.; Thakre, P. R.; Dong, H.; Patrick, J. F.; Vlasko-Vlasov, V. K.; Sottos, N. R.; Moore, J. S.; White, S. R. *Adv. Mater.* **2011**, *23*, 3654–3658.

(44) Patrick, J. F.; Hart, K. R.; Krull, B. P.; Diesendruck, C. E.; Moore, J. S.; White, S. R.; Sottos, N. R. *Adv. Mater.* **2014**, *26*, 4302–4308.

(45) Frischmann, P. D.; Gerber, L. C. H.; Doris, S. E.; Tsai, E. Y.; Fan, F. Y.; Qu, X.; Jain, A.; Persson, K. A.; Chiang, Y.-M.; Helms, B. A. *Chem. Mater.* **2015**, *27*, 6765–6770.

(46) Chen, Y.; Freunberger, S. A; Peng, Z.; Fontaine, O.; Bruce, P. G. *Nat. Chem.* **2013**, *5*, 489–494.

(47) Lim, H.-D.; Song, H.; Kim, J.; Gwon, H.; Bae, Y.; Park, K.-Y.; Hong, J.; Kim, H.; Kim, T.; Kim, Y. H.; Lepró, X.; Ovalle-Robles, R.; Baughman, R. H.; Kang, K. *Angew. Chem. Int. Ed.* **2014**, *53*, 3926–3931.

(48) Bergner, B. J.; Schürmann, A.; Peppler, K.; Garsuch, A.; Janek, J. *J. Am. Chem. Soc.* **2014**, *136*, 15054–15064.

(49) Feng, N.; He, P.; Zhou, H. *ChemSusChem* **2015**, *8*, 600–602.

(50) Lacey, M. J.; Frith, J. T.; Owen, J. R. *Electrochem. Commun.* **2013**, *26*, 74–76.

(51) Sun, D.; Shen, Y.; Zhang, W.; Yu, L.; Yi, Z.; Yin, W.; Wang, D.; Huang, Y.; Wang, J.; Wang, D.; Goodenough, J. B. *J. Am. Chem. Soc.* **2014**, *136*, 8941–8946.

(52) Xia, C.; Black, R.; Fernandes, R.; Adams, B.; Nazar, L. F. *Nat. Chem.* **2015**, *7*, 496–501.

(53) Zhang, S. S. *J. Power Sources* **2013**, *231*, 153–162.

(54) Wu, H.-L.; Huff, L. A.; Gewirth, A. A. *ACS Appl. Mater. Interfaces* **2015**, *7*, 1709–1719.

(55) Cuisinier, M.; Cabelguen, P.-E.; Evers, S.; He, G.; Kolbeck, M.; Garsuch, A.; Bolin, T.; Balasubramanian, M.; Nazar, L. F. *J. Phys. Chem. Lett.* **2013**, *4*, 3227–3232.

(56) Pascal, T. A; Wujcik, K. H.; Velasco-Velez, J. J.; Wu, C.; Teran, A. A.; Kapilashrami, M.; Cabana, J.; Guo, J.; Salmeron, M.; Balsara, N.; Prendergast, D. *J. Phys. Chem. Lett.* **2014**, *5*, 1547–1551.

(57) Wujcik, K. H.; Velasco-Velez, J.; Wu, C. H.; Pascal, T. A.; Teran, A. A.; Marcus, M. A.; Cabana, J.; Guo, J.; Prendergast, D.; Salmeron, M.; Balsara, N. P. *J. Electrochem. Soc.* **2014**, *161*, A1100–A1106.

(58) Meini, S.; Elazari, R.; Rosenman, A.; Garsuch, A.; Aurbach, D. *J. Phys. Chem. Lett.* **2014**, *5*, 915–918.

(59) Bard, A. J.; Faulkner, L. R. *Electrochemical Methods Fundamentals and Applications*, 2nd ed.; John Wiley and Sons, Inc: Hoboken, NJ, 2001; p 96.

(60) Kojima, H.; Bard, A. J. *J. Am. Chem. Soc.* **1975**, *97*, 6317–6324.

(61) Ruoff, R. S.; Kadish, K. M.; Boulas, P.; Chen, E. C. M. *J. Phys. Chem.* **1995**, *99*, 8843–8850.

(62) Peverati, R.; Truhlar, D. G. *J. Phys. Chem. Lett.* **2011**, *2*, 2810–2817.

(63) Perdew, J. P.; Burke, K.; Ernzerhof, M. *Phys. Rev. Lett.* **1996**, *77*, 3865–3868.

(64) Qu, X.; Jain, A.; Rajput, N. N.; Cheng, L.; Zhang, Y.; Ong, S. P.; Brafman, M.; Maginn, E.; Curtiss, L. A.; Persson, K. A. *Comput. Mater. Sci.* **2015**, *103*, 56–67.

(65) Cheng, L.; Assary, R. S.; Qu, X.; Jain, A.; Ong, S. P.; Rajput, N. N.; Persson, K.; Curtiss, L. A. *J. Phys. Chem. Lett.* **2015**, *6*, 283–291.

(66) Chen, Z.; Lohr, A.; Saha-Möller, C. R.; Würthner, F. *Chem. Soc. Rev.* **2009**, *38*, 564–584.

(67) De Greef, T. F. A.; Smulders, M. M. J.; Wolffs, M.; Schenning, A. P. H. J.; Sijbesma, R. P.; Meijer, E. W. *Chem. Rev.* **2009**, *109*, 5687–5754.

(68) Fan, F. Y.; Carter, W. C.; Chiang, Y.-M. *Adv. Mater.* **2015**, *27*, 5203–5209.

(69) Jafarian, M.; Mahjani, M. G.; Gobal, F.; Danaee, I. *J. Electroanal. Chem.* **2006**, *588*, 190–196.

(70) Fleischmann, M.; Thirsk, H. R. In *Advances in Electrochemistry and Electrochemical Engineering, Vol. 3*; Delahay, P., Ed.; John Wiley & Sons: New York, 1963; pp 123–210.

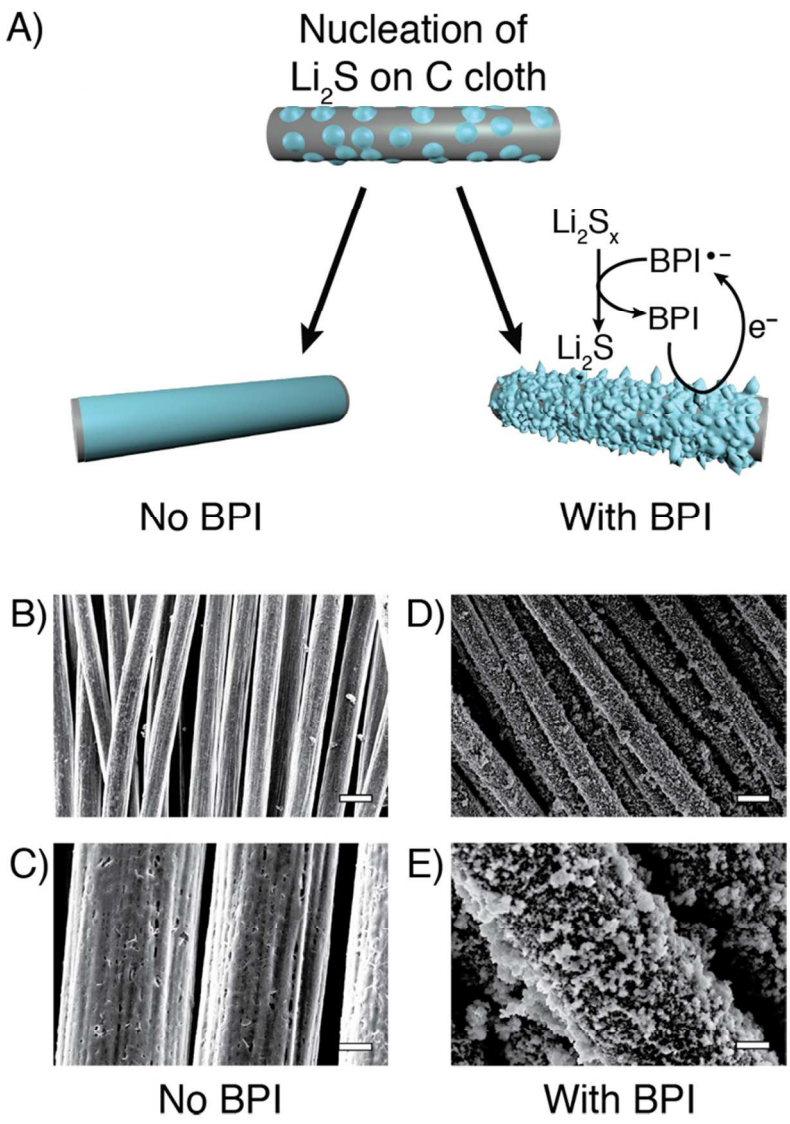

83x94mm (300 x 300 DPI)

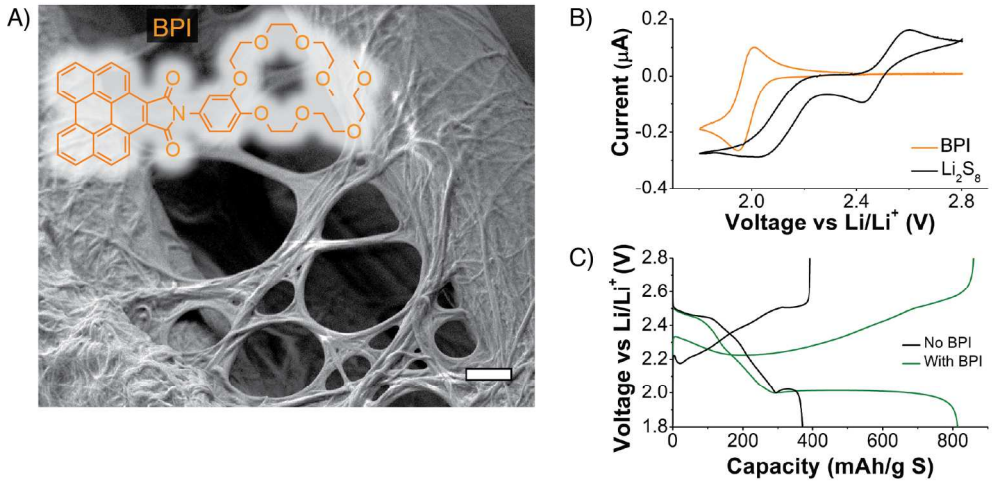

174x85mm (299 x 299 DPI)

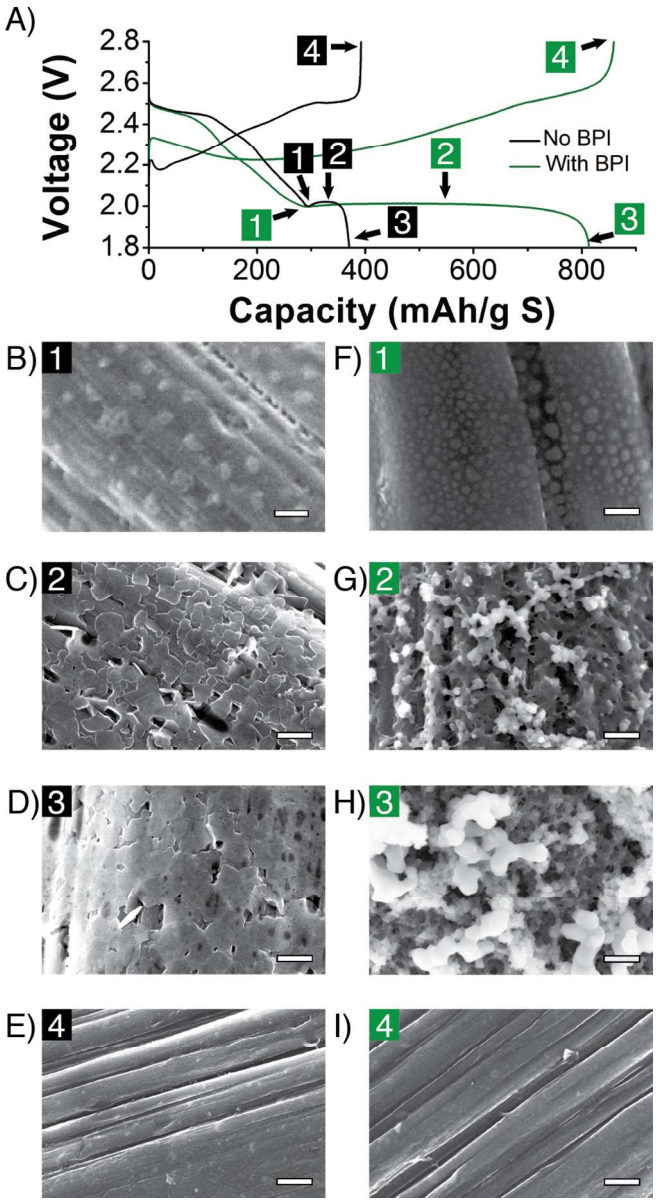

84x157mm (299 x 299 DPI)

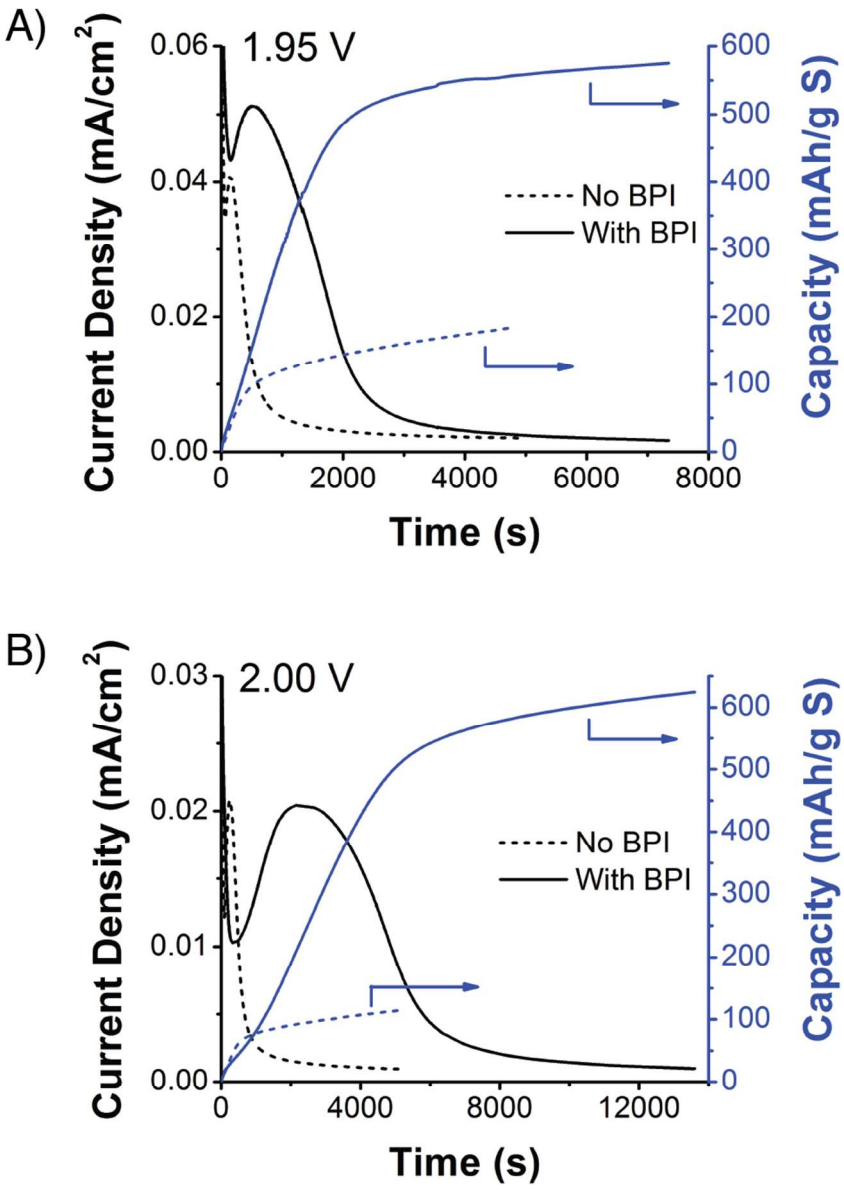

84x117mm (299 x 299 DPI)

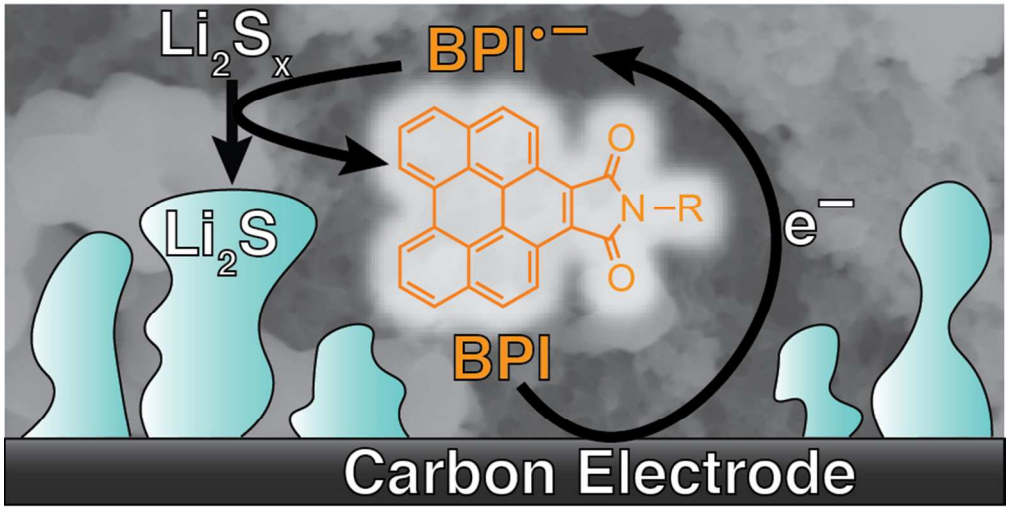

80x42mm (299 x 299 DPI)